Platelets guide the formation of early metastatic niches

Myriam Labelle[a,b,1], Shahinoor Begum[a], and Richard O. Hynes[a,1]

[a]Howard Hughes Medical Institute, Koch Institute for Integrative Cancer Research, Massachusetts Institute of Technology, Cambridge, MA 02139; and [b]Department of Developmental Neurobiology, St. Jude Children's Research Hospital, Memphis, TN 38105

Contributed by Richard O. Hynes, June 16, 2014 (sent for review April 24, 2014; reviewed by Yibin Kang and Michael H. Kroll)

During metastasis, host cells are recruited to disseminated tumor cells to form specialized microenvironments ("niches") that promote metastatic progression, but the mechanisms guiding the assembly of these niches are largely unknown. Tumor cells may autonomously recruit host cells or, alternatively, host cell-to-host cell interactions may guide the formation of these prometastatic microenvironments. Here, we show that platelet-derived rather than tumor cell-derived signals are required for the rapid recruitment of granulocytes to tumor cells to form "early metastatic niches." Granulocyte recruitment relies on the secretion of CXCL5 and CXCL7 chemokines by platelets upon contact with tumor cells. Blockade of the CXCL5/7 receptor CXCR2, or transient depletion of either platelets or granulocytes prevents the formation of early metastatic niches and significantly reduces metastatic seeding and progression. Thus, platelets recruit granulocytes and guide the formation of early metastatic niches, which are crucial for metastasis.

Interactions between host cells and tumor cells both at the primary and metastatic sites are crucial for efficient metastasis (1–3). At the site of metastasis, host cell–tumor cell cross talk contributes to the formation of a metastatic niche, a specialized microenvironment necessary for disease progression. Leukocytes, in particular monocytes and macrophages, have been shown to be recruited to metastatic niches and to support metastasis (4–10). Mechanistically, macrophages secrete VEGFA that facilitates tumor cell extravasation (4). In addition, interaction of monocytes/macrophages with tumor cells via VCAM1 can prevent tumor cell apoptosis and allow reinitiation of growth at the metastatic site (8, 9). Granulocytes have also been reported to interact with tumor cells and facilitate metastatic seeding possibly by enhancing tumor cell arrest and extravasation (11–13). However, granulocytes exposed to specific environmental stimuli can kill metastatic tumor cells, suggesting that their role in metastasis is highly context dependent (14, 15).

Platelets, which interact with tumor cells during their transit through the circulation, also enhance metastasis via multiple mechanisms (3, 16). Metastatic tumor cells can express high levels of tissue factor (TF) and adhesion molecules, such as P-selectin ligands, through which they bind to and activate platelets (16). These interactions result in the formation by platelets of a physical shield around tumor cells, which prevents attacks from natural killer (NK) cells and promotes tumor cell adhesion to the endothelium (17–19). In addition, platelets also promote tumor cell extravasation by increasing endothelial permeability and by directly signaling to tumor cells to enhance their invasive and metastatic potential (20, 21). In particular, direct contact between platelets and tumor cells triggers the TGFβ1 and NF-κB signaling pathways in tumor cells, which induce an epithelial–mesenchymal transition and promote metastasis (20). Given their important signaling roles, platelets may influence metastasis by signaling not only to tumor cells but also to host cells forming metastatic niches. Furthermore, whether platelets and leukocytes are independently recruited by cancer cells to the site of metastasis, or whether hierarchical interactions among host cells drive the formation of metastatic niches remains unknown. Here, we define the relative roles of platelets and leukocytes during the early stages of metastatic seeding and the subsequent impact of these interactions on metastatic progression.

Results

$CD11b^+MMP9^+Ly6G^+$ Granulocytes Are Recruited to Platelet–Tumor Cell Microthrombi to Form Early Metastatic Niches. To understand the role of the microenvironment during the early intravascular steps of the metastatic cascade, we first sought to determine which cell types are associated with tumor cells in the lungs of mice 2 h after tail vein injection, a time point at which tumor cells are arrested in capillaries and associated with platelets, but still localized intravascularly (18, 20). Immunofluorescence staining for platelets and leukocyte markers revealed the presence of prominent platelet aggregates in association with MC38GFP tumor cells (Fig. 1 *A* and *B*). Furthermore, an approximately fivefold increase in the number of cells coexpressing integrin alpha M (CD11b), the granulocyte marker Ly6G (22), and matrix metallopeptidase 9 (MMP9), another protein abundantly expressed by granulocytes (14, 23), was also observed (Fig. 1 *A* and *B* and Fig. S1*A*). Interestingly, $CD11b^+MMP9^+Ly6G^+$ cells were not simply globally enriched in the lungs, but were recruited specifically to the vicinity of platelet–tumor cell aggregates (Fig. 1 *A* and *B*). This specific recruitment was also observed when only few tumor cells were arrested in the lungs, revealing a significant increase in the number of granulocytes localized within 40 μm of platelet–tumor cell aggregates, compared with their normal distribution in control adjacent areas of the lungs of the same mouse (Fig. S1 *B* and *C*).

Significance

Specialized microenvironments (or "niches") are essential for metastasis, but how cancer cells and host cells contribute to their establishment remains poorly understood. Our study reveals that platelets and granulocytes are sequentially recruited to disseminated tumor cells to form "early metastatic niches" that promote metastatic progression. Importantly, the recruitment of granulocytes is not primarily due to tumor cell-derived signals but rather relies on platelet-derived CXCL5/7 chemokines. Prevention of granulocyte recruitment via inhibition of the CXCL5/7 receptor CXCR2, or depletion of either platelets or granulocytes inhibits metastasis, thereby uncovering a key role for platelet-to-granulocyte signaling in the establishment of metastases. Specific inhibition of platelet-to-granulocyte interactions may thus represent a valuable antimetastatic therapy in addition to cancer cell-centered treatments.

Author contributions: M.L. and R.O.H. designed research; M.L. and S.B. performed research; M.L. analyzed data; and M.L. and R.O.H. wrote the paper.

Reviewers: Y.K., Princeton University; and M.H.K., The University of Texas MD Anderson Cancer Center.

The authors declare no conflict of interest.

Freely available online through the PNAS open access option.

[1]To whom correspondence may be addressed. Email: rohynes@mit.edu or myriam.labelle@stjude.org.

This article contains supporting information online at www.pnas.org/lookup/suppl/doi:10.1073/pnas.1411082111/-/DCSupplemental.

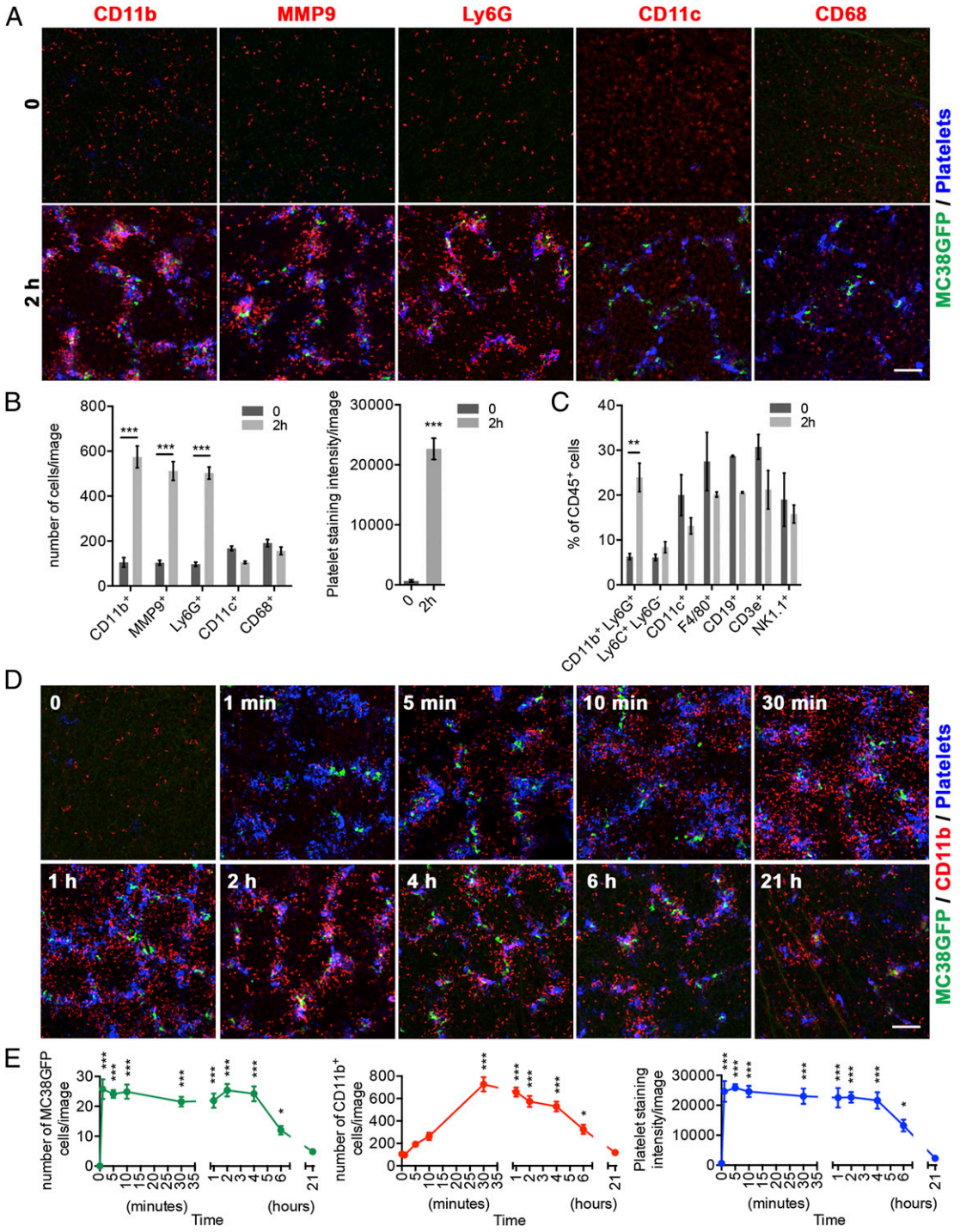

Fig. 1. CD11b$^+$MMP9$^+$Ly6G$^+$ granulocytes are recruited to platelet–tumor cell aggregates within 2 h of tumor cell entry into the circulation. (*A*) Immunostaining of lungs from control mice (0; no injection) or from mice killed 2 h after the injection of 10^6 MC38GFP tumor cells (green). Staining for the immune cell markers CD11b, MMP9, Ly6G, CD11c, or CD68 (red) reveals that CD11b$^+$, MMP9$^+$, and Ly6G$^+$ cells are recruited to the platelet (blue)–tumor cell (green) aggregates, whereas CD11c$^+$ and CD68$^+$ cells are not. Platelets were stained with an anti-GP1bβ antibody (blue). (Scale bar: 100 μm.) See Fig. S1 for CD11b, Ly6G, and MMP9 costaining. (*B*) Numbers of CD11b$^+$, MMP9$^+$, Ly6G$^+$, CD11c$^+$, and CD68$^+$ cells (*Left*), and intensity of platelet staining (*Right*) in lungs of mice treated as in *A*. Bars represent the mean ± SEM ($n \geq 12$ images from $n \geq 3$ mice). ***$P < 0.001$ was determined by unpaired two-sided *t* test. (*C*) Mouse lungs were collected at time 0 or 2 h after the injection of 10^6 MC38GFP tumor cells, and the percentages of different immune cell populations among total immune cells (CD45$^+$) were determined by FACS. Bars represent the mean ± SEM ($n \geq 3$ mice). **$P < 0.01$ was determined by unpaired two-sided *t* test. (*D*) Time course of the formation of the early metastatic niche. Immunostaining for CD11b (red), and platelets (GP1bβ; blue) in mouse lungs at the times indicated following the injection of 10^6 MC38GFP cells (green). Platelet–tumor cell aggregates are formed within 1 min of MC38GFP cell entry into the circulation. In comparison, the recruitment of CD11b$^+$ cells (red) to the platelet–tumor cell aggregates requires 30 min to 4 h. Note the clear enrichment for CD11b$^+$ cells in the vicinity of tumor cells at 2 and 4 h. (Scale bar: 100 μm.) (*E*) Numbers of MC38GFP tumor cells (*Left*) and CD11b$^+$ cells (*Center*), and intensity of platelet staining (*Right*) in mouse lungs collected at the times indicated following the injection of MC38GFP cells. Points represent the mean ± SEM ($n \geq 12$ images from $n \geq 3$ mice). Statistical significance for values at each time point compared with time 0 was determined by one-way ANOVA followed by Tukey's post test (*$P < 0.05$ and ***$P < 0.001$). See also Fig. S1.

No $CD11b^+$ cell recruitment was observed when only vehicle (HBSS) was injected (Fig. S1 *D* and *E*). In addition, no changes in the total number or spatial distribution of $CD11c^+$ cells (dendritic cells and alveolar macrophages) and $CD68^+$ cells (macrophages) were observed 2 h after tumor cell injection (Fig. 1 *A* and *B*). Further analysis by flow cytometry (Fig. 1*C*) confirmed the enrichment of $CD11b^+Ly6G^+$ granulocytic cells (which are also positive for $Gr1^+$; Fig. S1*F*) in the lungs of mice injected with tumor cells, whereas no increases in the numbers of $Ly6C^+Ly6G^-$ monocytes, $CD11c^+$ macrophages and dendritic cells, $F4/80^+$ macrophages, $CD19^+$ B lymphocytes, $CD3\varepsilon^+$ T lymphocytes, or $NK1.1^+$ NK cells were observed (Fig. 1*C*). Overall, these results demonstrate that, together with platelets, $CD11b^+MMP9^+Ly6G^+$ granulocytes are a major component of the metastatic niche at this early time point.

To define the sequential events leading to the formation of the early metastatic niche, the cellular interactions occurring during the first 2 h following tumor cell injection were monitored over time. Platelet aggregates surrounding tumor cells were present in the lungs of mice 1 min after the injection of tumor cells, but no recruitment of granulocytes was yet observed (Fig. 1 *D* and *E*), demonstrating that platelet–tumor cell interactions are induced very rapidly and suggesting that they are triggered while tumor cells circulate, or immediately upon their initial trapping in the lungs. Subsequently, granulocytes were progressively recruited to platelet–tumor cell aggregates over the next 30 min, with no further changes in their association from 30 min to 4 h. At 6 h postinjection, the platelet aggregates around tumor cells were smaller and there were fewer granulocytes in the lungs compared with the 2-h time point, indicating that these transient interactions were progressively dismantled. At 21 h, a time point at which tumor cells have started to extravasate (20), the association of platelets with tumor cells was minimal and the numbers of granulocytes in the lungs similar to baseline. Thus, these data reveal that the very rapid formation of platelet–tumor cell aggregates is followed by the progressive recruitment of granulocytes to generate a transient early metastatic niche.

Platelets Are Required for the Recruitment of Granulocytes to the Early Metastatic Niche. Because platelet–tumor cell aggregates are formed before the recruitment of granulocytes (Fig. 1 *D* and *E*), we next tested whether platelets could influence the formation of the early metastatic niche. Remarkably, platelet depletion via injection of a platelet-depleting antibody had no effect on the number of tumor cells arrested in the lungs but led to a complete inhibition of the recruitment of granulocytes to tumor cells (Fig. 2 *A* and *B* and Fig. S2*A*). Similarly, the recruitment of granulocytes was also greatly reduced in integrin β3-null (*Itgb3*$^{-/-}$) mice, which have impaired platelet aggregation compared with wild-type mice (24) (Fig. 2 *C* and *D* and Fig. S2*B*). To further test the requirement for platelets in the recruitment of granulocytes to tumor cells, we injected Chinese hamster ovary (CHO) cells, which do not have the capacity to induce the formation of platelet aggregates (25). Although numerous CHO cells arrested in the lungs 2 h postinjection, no substantial platelet–tumor cell aggregates were formed, and the recruitment of granulocytes was also inhibited (Fig. 2 *E* and *F* and Fig. S2*C*). In contrast, similarly to our observations with MC38GFP cells, injection of Lewis lung carcinoma (LLC) cells or of melanoma (B16F10) cells resulted in the formation of platelet–tumor cell aggregates and in granulocyte recruitment, indicating that the formation of the early metastatic niche is a general response to multiple types of tumor cells (Fig. S2*D*). Taken together, these results indicate that platelets do not affect the initial arrest of tumor cells in the lung capillaries. However, efficient formation of platelet–tumor cell aggregates is crucial for the subsequent recruitment of granulocytes to the early metastatic niche, and tumor cells per se are not sufficient to trigger this recruitment.

Platelet-Induced Recruitment of Granulocytes Promotes Metastasis. Granulocytes may either inhibit or promote tumor progression and metastasis depending on the microenvironmental cues to which they are exposed (7, 10, 11, 14, 15). To test whether the recruitment of granulocytes to platelet–tumor cell aggregates influences the subsequent formation of metastases, we treated mice with a single dose of anti-Ly6G or anti-Gr1 granulocyte-depleting antibodies 24 h before the injection of MC38GFP tumor cells and monitored the resulting effects after 2 h (Fig. 3 *A*–*C*), 48 h (Fig. 3*D*), and 14 d (Fig. 3*E*). Both antibodies effectively depleted granulocytes in lungs as observed 2 h after the injection of tumor cells but did not affect the platelet–tumor cell aggregates nor the number of tumor cells found in the lungs (Fig. 3 *A*–*C*). Importantly, fewer metastases were observed in mice treated with a single dose of either the anti-Ly6G or anti-Gr1 granulocyte-depleting antibodies (Fig. 3*E*, *Left* and *Center*), demonstrating that granulocytes play an important supportive role during the early steps of metastatic progression. Indeed, proportional reductions in the numbers of tumor cells retained in the lungs after 48 h were observed (Fig. 3*D*, *Left* and *Center*), indicating that granulocytes contribute to the formation of a microenvironment that is favorable for metastatic cell seeding. In line with previous observations (17, 26, 27), platelet depletion led to an almost complete inhibition of tumor cell seeding after 48 h, and of overt metastatic burden after 14 d (Fig. 3 *D* and *E*, *Right*). The more potent effect of platelet depletion compared with granulocyte depletion is consistent with platelets playing a variety of prometastatic roles and promoting metastasis not only via the recruitment of granulocytes, but also via additional mechanisms (3, 16). Taken together, these results indicate that platelet–tumor cell interactions are essential for the subsequent recruitment of granulocytes, which in turn further support metastatic seeding. Thus, the recruitment of granulocytes represents an important prometastatic function of platelets.

Platelet-Derived Factors Are Chemotactic for Granulocytes. We then aimed to define further the mechanisms involved in the platelet-mediated recruitment of granulocytes to the early metastatic niche. Imaging and 3D rendering revealed that, whereas granulocytes are enriched in the vicinity of platelet–tumor cell aggregates, many granulocytes are not in direct contact with either platelet aggregates or tumor cells (Fig. 4*A*), suggesting that their recruitment is not due to their physical trapping/adhesion to platelet–tumor cell aggregates, but rather to chemotactic factors. To test this hypothesis, we performed in vitro leukocyte migration assays where platelets and tumor cells (either individually or in combination) were used as sources of chemoattractants. Interestingly, whereas platelets or tumor cells alone did not induce significant migration of $CD11b^+Ly6G^+$ granulocytes compared with buffer, coincubating platelets with MC38GFP tumor cells led to a significant increase in granulocyte migration (Fig. 4*B*). Furthermore, this chemotactic effect could be recapitulated by conditioned medium (supernatant) from platelets coincubated with MC38GFP cells, but not by the combination of conditioned media obtained from these two individual sources, demonstrating that direct interaction between platelets and MC38GFP tumor cells is required for the release/secretion of chemoattractants that promote the recruitment of granulocytes. Because direct contact between platelets and tumor cells induces platelet activation (28, 29), we next tested whether the chemotactic factors are released as a result of platelet activation, or whether chemotactic factors contributed by tumor cells are also involved. The supernatant from thrombin-activated platelets induced a similar increase in granulocyte migration as observed with platelets plus MC38GFP cells (Fig. 4*C*). Furthermore, adding MC38GFP cells to the supernatant from thrombin-activated platelets did not further increase granulocyte recruitment (Fig. 4*C*), indicating that the chemotactic

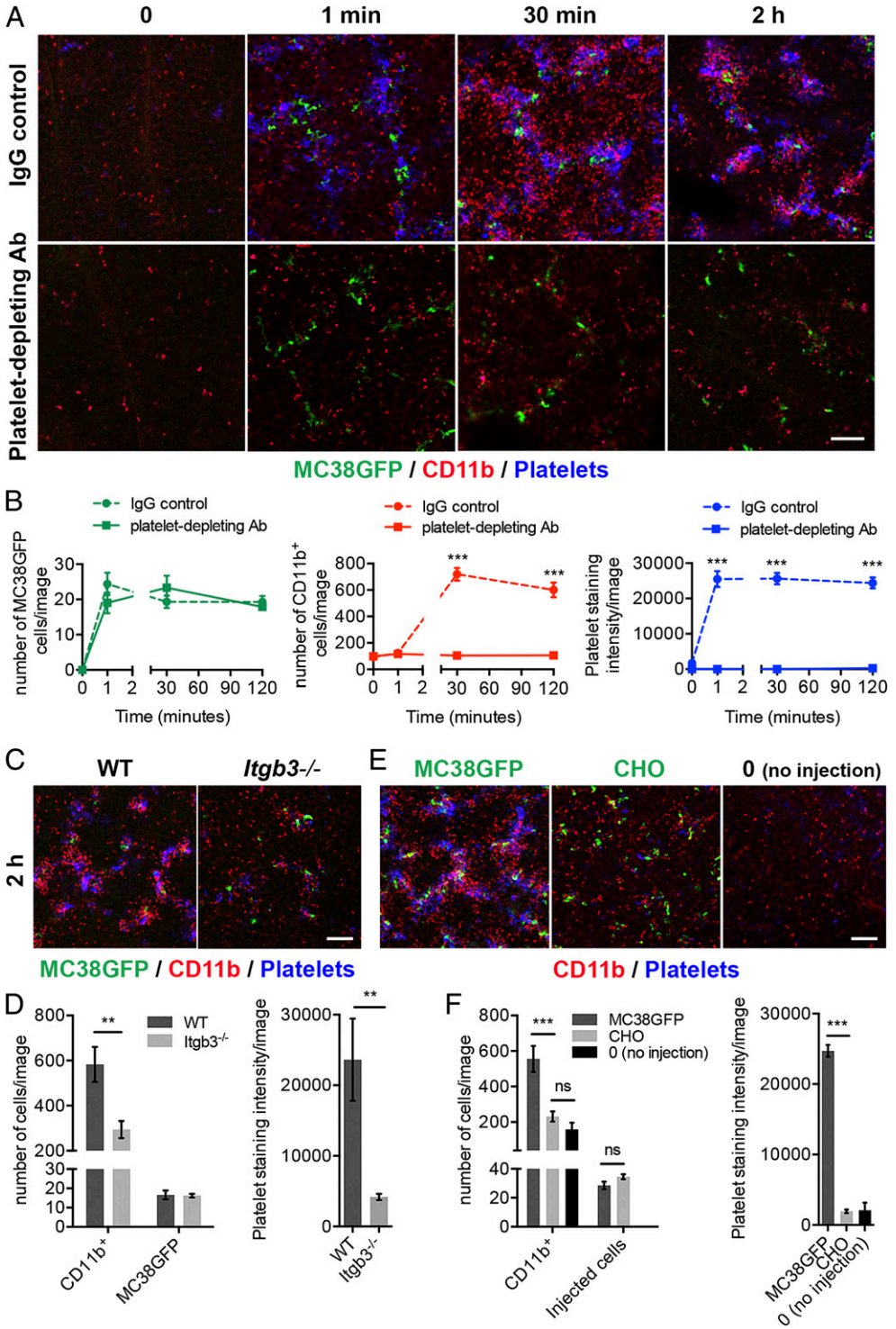

Fig. 2. Platelets are required for the recruitment of granulocytes to the early metastatic niche but not for the initial arrest of tumor cells. (*A*) Platelet depletion inhibits the recruitment of CD11b$^+$ cells to the lungs. Mice were treated with a platelet-depleting antibody (anti-GP1bα) or an IgG control 24 h before the i.v. injection of MC38GFP cells. Immunostaining for CD11b (red), and platelets (GP1bβ; blue) in mouse lungs at the times indicated following the injection of MC38GFP cells (green). (Scale bar: 100 μm.) (*B*) Numbers of MC38GFP cells (*Left*) and CD11b$^+$ cells (*Center*), and intensity of platelet staining (*Right*) in lungs of mice treated as in *A*. Points represent the mean ± SEM ($n \geq 21$ images from $n \geq 4$ mice). Statistical significance for platelet-depleting antibody treatment vs. IgG control at each time point was determined by unpaired two-sided *t* test (***$P < 0.001$). (*C*) Immunostaining for CD11b (red) and platelets (GP1bβ; blue) in lungs from wild-type (WT) or *Itgb3*$^{-/-}$ mice 2 h after the injection of MC38GFP cells (green). (Scale bar: 100 μm.) (*D*) Numbers of CD11b$^+$ cells and MC38GFP cells (*Left*), and intensity of platelet staining (*Right*) in lungs of mice treated as in *C*. Bars represent the mean ± SEM ($n \geq 12$ images from $n \geq 3$ mice). **$P < 0.01$ was determined by unpaired two-sided *t* test. (*E*) Immunostaining for CD11b (red) and platelets (GP1bβ; blue) in lungs from NOD SCID mice 2 h after the injection of MC38GFP or CellTracker Green-labeled CHO cells (green). Lungs of control (0; no injection) NOD SCID mice are also shown. (Scale bar: 100 μm.) (*F*) Numbers of CD11b$^+$ cells and MC38GFP cells (*Left*), and intensity of platelet staining (*Right*) in lungs of mice treated as in *E*. Bars represent the mean ± SEM ($n \geq 12$ images from $n \geq 3$ mice). ***$P < 0.001$ and ns ($P > 0.05$) were determined by unpaired two-sided *t* test. See also Fig. S2.

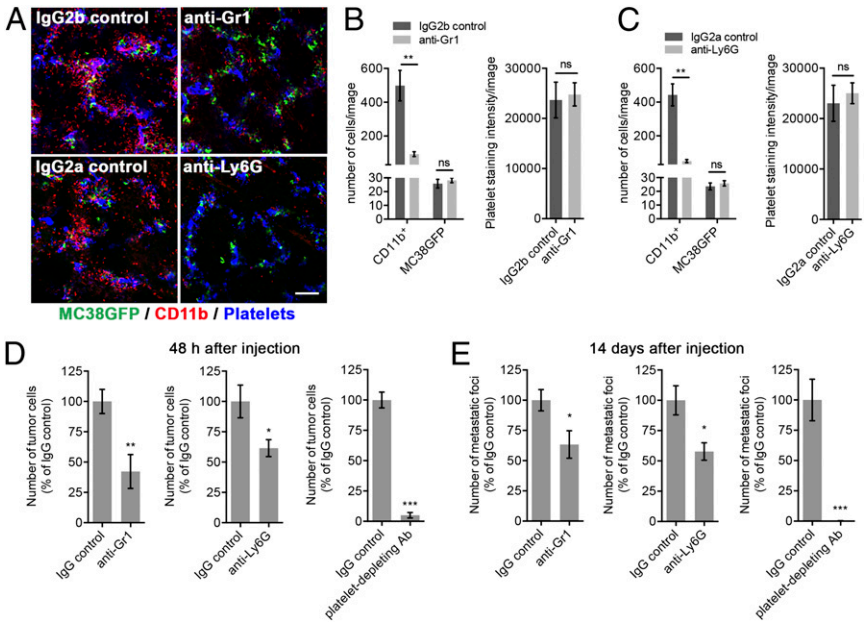

Fig. 3. Granulocytes and platelets promote metastasis. (*A*) Mice were treated with anti-Gr1, anti-Ly6G, or IgG controls 24 h before the i.v. injection of MC38GFP cells. Immunostaining for CD11b (red), and platelets (GP1bβ; blue) in mouse lungs 2 h after the injection of MC38GFP cells (green). (Scale bar: 100 μm.) (*B* and *C*) Numbers of $CD11b^+$ cells and MC38GFP cells (*Left*), and intensity of platelet staining (*Right*) in lungs of mice treated as in *A*. Bars represent the mean ± SEM ($n \geq 12$ images from $n \geq 3$ mice). $^{**}P < 0.01$ and ns ($P > 0.05$) were determined by unpaired two-sided *t* test. (*D*) Numbers of tumor cells at the surface of lungs 48 h after tail vein injection of MC38GFP cells in mice pretreated with anti-Gr1 (*Left*), anti-Ly6G (*Center*), or platelet-depleting antibodies (*Right*), compared with their respective IgG controls. Bars represent the mean ± SEM ($n = 5$ mice). $^{*}P < 0.05$, $^{**}P < 0.01$, and $^{***}P < 0.001$ were determined by unpaired two-sided *t* test. (*E*) Numbers of metastatic foci at the surface of lungs (two largest lobes) 14 d after tail vein injection of MC38GFP cells in mice pretreated with anti-Gr1 (*Left*), anti-Ly6G (*Center*), or platelet-depleting antibodies (*Right*), compared with their respective IgG controls. Bars represent the mean ± SEM ($n = 7$ mice). $^{*}P < 0.05$ and $^{***}P < 0.001$ were determined by unpaired two-sided *t* test.

factors are provided by activated platelets rather than by MC38GFP tumor cells.

To identify chemotactic factors released by platelets upon their activation by direct contact with MC38GFP tumor cells, we used antibody arrays to monitor the expression of 96 chemokines and soluble factors. Three of the five soluble factors with highest staining intensities (CXCL2, CXCL5, and CXCL7) were members of the ELR^+ CXC chemokine family (CXCR2 ligands) (Fig. 4 *D* and *E* and Table S1). Among these five secreted factors, the concentrations of CXCL5 and CXCL7 were significantly increased in supernatant from platelets plus MC38GFP compared with supernatant from platelets or MC38GFP alone (Fig. 4*E*), whereas no significant increase was detected for the other three soluble factors highly expressed by platelets. To test whether the increase in granulocyte chemotaxis toward platelet-plus-MC38GFP cocultures or thrombin-activated platelets is dependent on either CXCL5 or CXCL7, blocking antibodies were added to the platelet-plus-MC38GFP cocultures or to thrombin-activated platelets. Interestingly, simultaneous blockade of both CXCL5 and CXCL7 led to a marked reduction in the number of granulocytes migrating toward platelets plus MC38GFP cells or thrombin-activated platelets, whereas individual blockade of either of these chemokines had no effect (Fig. 4*F*). Furthermore, MC38GFP cells expressed very low levels of CXCR2 ligands (CXCL1/2/5/7) in comparison with platelets (Fig. 4 *D* and *E* and Table S1), further indicating that platelets are the main source of CXCR2 ligands in this context. Thus, two platelet-derived chemokines, CXCL5 and CXCL7, which are abundantly released upon tumor cell-induced platelet activation, are crucial mediators of granulocyte recruitment in vitro. Given that CXCL7 is one of the most abundant platelet chemokines and that its expression is mostly restricted to platelets (30, 31), platelets may therefore possess a particular ability to potently attract granulocytes to the early metastatic niche.

Blocking Platelet-to-Granulocyte Signaling Prevents the Formation of the Early Metastatic Niche and Impairs Subsequent Metastasis. Because both CXCL5 and CXCL7 are ligands for the granulocyte receptor CXCR2, which mediates ELR^+ CXC chemokine-dependent granulocyte recruitment to sites of inflammation (32), we further tested whether inhibition of the CXCL5/7–CXCR2 signaling axis would prevent the formation of the early metastatic niche and therefore block metastasis. Pretreating leukocytes with an anti-CXCR2 blocking antibody inhibited their migration toward platelet plus MC38GFP cells in vitro (Fig. 5*A*). Furthermore, the recruitment of granulocytes to platelet–tumor cell aggregates was inhibited in mice treated with a single dose of anti-CXCR2 blocking antibody 1 h before the injection of tumor cells (Fig. 5 *B* and *C*), demonstrating the involvement of CXCR2 signaling in the assembly of the early metastatic niche. The anti-CXCR2 blocking antibody treatment also led to a significant reduction in the number of tumor cells seeded in the lungs after 2 d and in the number of metastases observed after 14 d (Fig. 5 *D* and *E*), further demonstrating the importance of granulocyte recruitment for metastasis. Taken together, these results indicate a fundamental role of platelet–granulocyte interactions and of the CXCL5/7–CXCR2 axis in the formation of the early metastatic niche and in supporting efficient metastasis (Fig. 6).

Discussion

Here, we define an "early metastatic niche" that forms within 2 h of tumor cell initial arrest in the lung vasculature and that is characterized by the gradual and directed recruitment of granulocytes specifically to platelet–tumor cell aggregates (Fig. 1). No significant recruitment of monocytes, dendritic cells, NK cells, or lymphocytes to this early niche was observed, indicating that interactions between tumor cells, platelets and granulocytes dominate this intravascular stage of the metastatic cascade. The early metastatic niche is thus distinct from the prometastatic

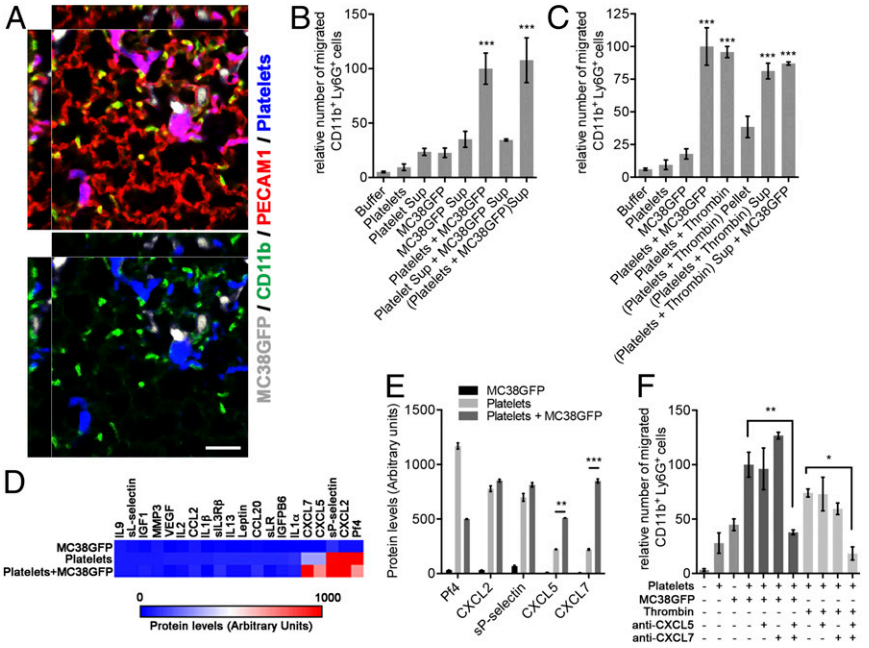

Fig. 4. Platelet-derived CXCL5 and CXCL7 are chemotactic factors for $CD11b^+Ly6G^+$ granulocytes. (*A*) Immunostaining for CD11b (green), platelets (GP1bβ; blue), and the endothelium (PECAM1; red) in mouse lungs 2 h after the injection of 10^6 MC38GFP cells (white). Note that $CD11b^+$ cells are enriched in the vicinity of the platelet–tumor cell aggregates, but are not necessarily in direct contact with platelet–tumor cell aggregates. (Scale bar: 50 μm.) (*B* and *C*) Numbers of $CD11b^+Ly6G^+$ cells that migrated toward the indicated chemoattractants after 2 h. Bars represent the mean ± SEM ($n = 3$). $^{***}P < 0.001$ vs. buffer was determined by one-way ANOVA followed by Tukey's post test. Sup indicates centrifugation supernatants (conditioned media) from either platelets, MC38GFP, platelets-plus-MC38GFP coculture, or platelets activated with thrombin. (*D*) Heat map of chemokines and cytokines protein levels determined with antibody arrays incubated with supernatants from platelets, MC38GFP cells, or platelets plus MC38GFP. The 20 factors with the highest staining intensities are shown. See Table S1 for a complete list of chemokines and cytokines assayed and their staining intensities. (*E*) Protein expression levels for the five most abundant secreted factors determined in *D*. Bars represent the mean ± SEM. $^{**}P < 0.01$ and $^{***}P < 0.001$ were determined by one-way ANOVA followed by Tukey's post test. (*F*) Numbers of $CD11b^+Ly6G^+$ cells that migrated toward the indicated chemoattractants after 2 h. Bars represent the mean ± SEM ($n = 3$). $^{*}P < 0.05$ and $^{**}P < 0.01$ were determined by one-way ANOVA followed by Tukey's post test.

monocyte/macrophage–tumor cell interactions, which are typically observed between 8 and 48 h after tumor cell entry into the circulation, and which therefore likely characterize subsequent steps of the metastatic cascade (4, 6, 33).

Importantly, the recruitment of granulocytes to the early metastatic niche is strictly dependent on platelet activation and is blocked if platelets fail to aggregate around tumor cells either due to defective platelet function, to reduced numbers of circulating platelets, or to the intrinsic properties of tumor cells (Fig. 2). These data imply that (*i*) tumor cell-derived signals are unable to independently trigger the recruitment of granulocytes and that (*ii*) platelets are positioned upstream of granulocytes in the hierarchy of host cell interactions leading to the formation of the early metastatic niche. Indeed, our results indicate that granulocytes are actively recruited by platelet-derived CXCL5/7 chemokine signaling via the granulocyte receptor CXCR2. Therefore, the key signaling factors governing the recruitment of granulocytes to the early metastatic niche are primarily platelet derived rather than tumor cell derived. In breast cancer models, CXCL1 and CXCL2 produced by tumor cells during chemotherapy have been shown to recruit granulocytes to primary tumors (34). These two chemokines share the CXCR2 receptor with the CXCL5/7 ligands studied here. Collectively, these data and our findings thus suggest that distinct sets of CXCR2 ligands control the recruitment of granulocytes at different stages of tumor progression and of the metastatic cascade.

Despite the transient nature of the early metastatic niche (Fig. 1), its assembly is crucial for efficient metastatic progression. Both platelets and recruited granulocytes enhance metastatic seeding, as illustrated by the reduced number of cells retained in the lungs upon transient depletion of either platelets or granulocytes, or upon inhibition of granulocyte recruitment by anti-CXCR2 treatment (Figs. 3 and 5). However, platelet depletion results in a more potent inhibition of metastasis than granulocyte depletion alone, indicating that, in accordance with the multiple contributions of platelets to the early steps of the metastatic cascade (3, 16), their prometastatic role is not restricted to recruiting granulocytes. Granulocyte recruitment is nonetheless an important aspect of the prometastatic function of platelets and may therefore be a crucial component of the niche allowing for efficient progression to the next phases of the metastatic cascade. For example, granulocytes have been shown to promote transendothelial migration of tumor cells in vitro and tumor cell retention in the lungs at 24 h after tumor cell injection (11). Furthermore, the addition of granulocytes to platelets and tumor cells results in endothelial activation in vitro (6). In turn, the activated endothelium favors monocyte recruitment and adhesion in the vicinity of tumor cells (6, 35). On this basis, our data raise the possibility that the recruitment of monocytes observed in response to thrombus formation around tumor cells might not only directly depend on coagulation but also involve granulocytes (33). In this respect, it would be interesting to define the impact of prolonged or late-onset granulocyte depletion on host–tumor cell interactions and on metastasis.

Our findings suggest that specific inhibition of platelet-derived signals or platelet–granulocyte interactions might limit metastatic progression by preventing the formation of the early metastatic niche and be a valuable therapeutic alternative to cancer cell-centered antimetastatic approaches. The rationale for targeting the platelet–granulocyte interactions described in this study is supported by a number of recent clinical studies showing that high levels of serum CXCL5 (36) and elevated numbers of circulating

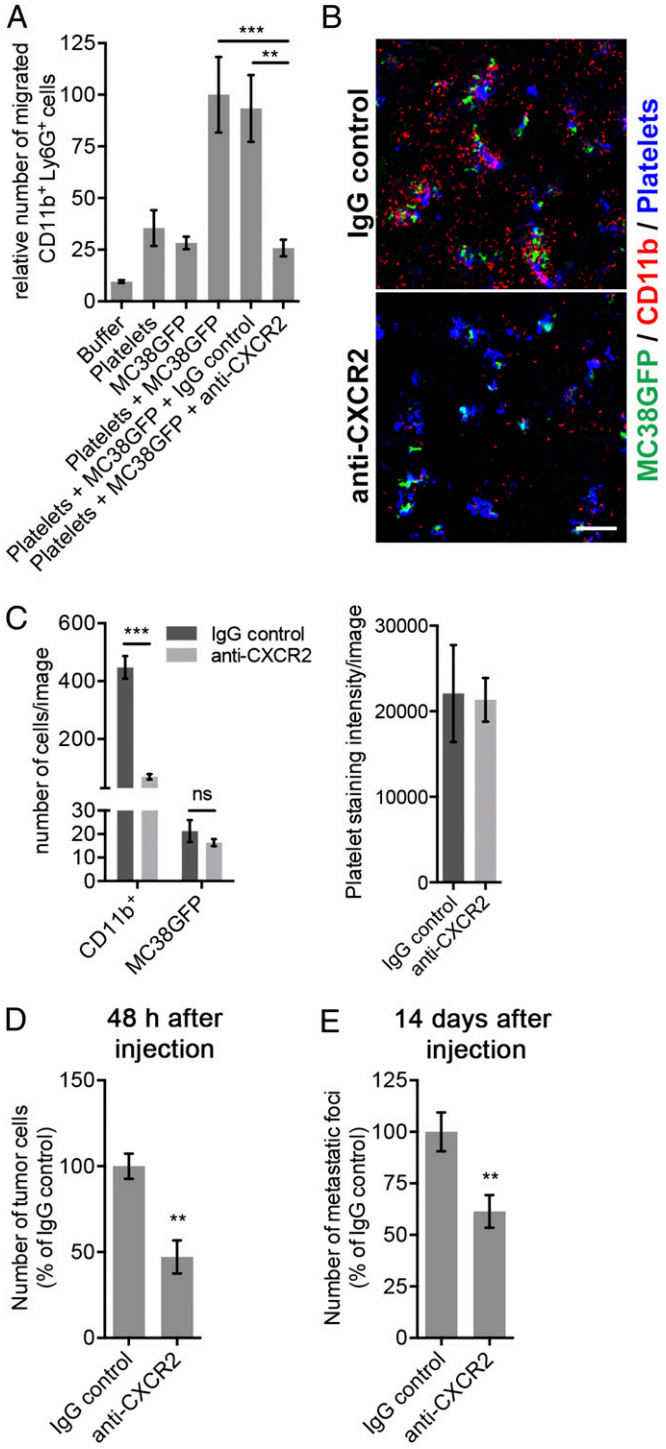

Fig. 5. Blocking the CXCR2 receptor prevents the formation of the early metastatic niche and inhibits subsequent metastasis. (*A*) Numbers of $CD11b^+$ $Ly6G^+$ cells that migrated toward the indicated chemoattractants after 2 h. Bars represent the mean ± SEM ($n = 3$). $^{**}P < 0.01$ and $^{***}P < 0.001$ were determined by one-way ANOVA followed by Tukey's post test. (*B*) Mice were treated with anti-CXCR2 or IgG control 1 h before the i.v. injection of MC38GFP cells. Immunostaining for CD11b (red), and platelets (GP1bβ; blue) in mouse lungs 2 h after the injection of MC38GFP cells (green). (Scale bar: 100 μm.) (*C*) Numbers of $CD11b^+$ cells and MC38GFP cells (*Left*), and intensity of platelet staining (*Right*) in lungs of mice treated as in *B*. Bars represent the mean ± SEM ($n \geq 12$ images from $n \geq 3$ mice). $^{***}P < 0.001$ and ns ($P > 0.05$) were determined by unpaired two-sided *t* test. (*D*) Numbers of tumor cells at the surface of lungs 48 h after tail vein injection of MC38GFP cells in mice pretreated with anti-CXCR2 or IgG control. Bars represent the mean ± SEM ($n = 5$ mice). $^{**}P < 0.01$ was determined by unpaired two-sided *t* test. (*E*) Numbers of metastatic foci at the surface of lungs 14 d after tail vein injection of MC38GFP cells in mice pretreated with anti-CXCR2 or IgG control. Bars represent the mean ± SEM ($n = 8$ mice). $^{**}P < 0.01$ was determined by unpaired two-sided *t* test.

granulocytes (37–42) are independent predictors of disease progression and adverse prognosis in cancer patients. Furthermore, our data suggest that these clinical observations might be mechanistically related to the well-known association of elevated platelet counts and platelet activation with poor prognosis (43–50).

Our study also indicates that pharmacological antagonists of CXCR2 may prevent the establishment of metastases by impairing signaling from platelet-derived CXCL5/7 and the formation of the early metastatic niche. However, given the involvement of CXCR2 and its ligands in granulocyte recruitment during antimicrobial host defense, anti-CXCR2 therapies may not be appropriate for individuals who are susceptible to infections (32). Nevertheless, CXCR2 inhibitors are currently being evaluated in the clinic for the treatment of inflammatory diseases and seem well tolerated by most patients (32, 51). In the context of cancer, CXCR2 inhibitors have been proposed to reduce the recruitment of granulocytes, angiogenesis, and tumor cell survival and invasion at the primary tumor site (32, 34, 52, 53). Taken together, these studies and our findings suggest that anti-CXCR2 therapies might be effective against both primary tumors as well as metastatic seeding by simultaneously targeting signaling from multiple CXCR2 ligands involved in cancer progression.

In conclusion, we highlight a hierarchical network of host cell interactions, which is necessary for the formation of the early metastatic niche and for efficient subsequent metastasis. Our results position platelets at the core of this hierarchical network and identify the CXCL5/7–CXCR2 signaling axis as a potential target for antimetastatic therapies.

Methods

Mice. Mouse colon carcinoma cells (MC38GFP; obtained from A. Varki, University of California, San Diego, CA), LLC cells, or melanoma cells (B16F10) were injected into 8- to 12-wk-old syngeneic wild-type (WT) or $Itgb3^{-/-}$ C57BL/6 mice (B6.129S2-Itgb3^{tm1Hyn}) (24). CHO cells and control MC38GFP cells were injected into 8- to 12-wk-old NOD/SCID mice (The Jackson Laboratory). For platelet depletion experiments, mice were injected via the tail vein with a single dose of platelet-depleting antibody (anti-GP1bα) or IgG control (50 μg per mouse; R300; Emfret) 24 h before the injection of tumor cells. This treatment leads to a greater than 95% reduction in platelet counts, which is achieved within 60 min of antibody injection and maintained for at least 48 h (54–56). To deplete $Ly6G^+$ cells, anti-Gr1 (RB6-8C5; BioLegend), anti-Ly6G (1A8; BioLegend), or IgG controls were administered by i.p. injection (50 μg per mouse) 24 h before tumor cells (22). Anti-mouse CXCR2 blocking antibody (MAB2164; R&D Systems) was injected at 150 μg per mouse via the tail vein 1 h before the injection of tumor cells. All mice were housed and handled in accordance with approved Massachusetts Institute of Technology Division of Comparative Medicine and St. Jude Children's Research Hospital Institutional Animal Care and Use Committee protocols.

In Vivo Lung Seeding and Metastasis Assays. For lung seeding and metastasis assays, cell lines were cultivated in DMEM, 10% (vol/vol) FCS, and 1% penicillin/streptomycin, and were subsequently trypsinized (LLC, B16F10, and CHO cells) or lifted with 2 mM EDTA in PBS (MC38GFP cells), washed, and resuspended in HBSS at 10^6 cells per 100 μL, unless otherwise indicated. One hundred microliters of cell suspension were then injected into mice via the tail vein. Mice were killed at the indicated time points and lungs were processed for imaging or FACS analysis. After 14 d, the numbers of metastatic foci at the surface of lungs (two biggest lobes) were counted under a fluorescence stereomicroscope. To quantify the seeding of tumor cells in the lungs after 48 h, four or more images of the surface of the lungs were taken (magnification, 3×) and the number of cells per image was automatically counted with Cell Profiler (57).

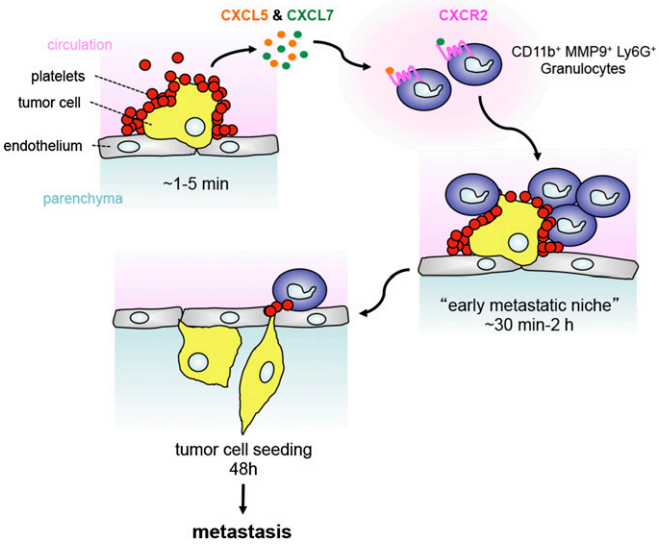

Fig. 6. Platelet-derived CXCL5 and CXCL7 chemokines guide the formation of the early metastatic niche. Platelet–tumor cell aggregates form very rapidly and localize to the site of initial arrest within 1 min of tumor cell entry into the circulation. Upon contact with tumor cells, platelets are activated and release CXCL5 and CXCL7 chemokines, which both signal via the CXCR2 receptor to recruit granulocytes to platelet–tumor cell aggregates, forming an early metastatic niche within the next hours. Preventing host–tumor cell interactions by interfering with platelet function or granulocyte recruitment impairs tumor cell seeding and metastasis, demonstrating the crucial supportive role of the early metastatic niche for subsequent metastatic progression.

Immunofluorescence Staining and Image Analysis. Lungs were fixed by tracheal perfusion with PBS with 4% (vol/vol) formaldehyde and 0.3% Triton X-100 for 15 min and removed en bloc. Lung lobes were then cut into small pieces, washed in PBS with 0.3% Triton X-100, and blocked in PBS with 10% (vol/vol) normal rabbit serum and 0.3% Triton X-100. The samples were then incubated with the primary antibodies [anti-mouse MMP9 (AF909; R&D Systems), CD11b (M1/70; BioLegend), Ly6G (1A8; BioLegend), CD68 (FA-11; BioLegend), CD11c (HL3; BD Biosciences), PECAM1 (MEC13.3; BD Biosciences)]. After washing, samples were incubated with secondary antibodies [Alexa 555-, 594-, or 647-conjugated goat anti-rat IgG, Alexa 555-, 594-, or 647-conjugated donkey anti-goat IgG (all from Invitrogen)], followed by additional washing and incubation with fluorophore-conjugated antibodies [anti-mouse CD11b, GP1bβ (X649; Emfret)]. Images were taken at 10× with a Nikon A1R inverted confocal microscope. The numbers of MC38GFP cells and $CD11b^+$ cells per image and the intensity of platelet staining were quantified with CellProfiler. For *XYZ* views, images were taken at 40× with *Z* sections every 1 μm, and *XYZ* views were generated with NIS-Elements (Nikon) and Volocity (Perkin-Elmer).

To determine the number of cells within 40 μm of MC38GFP cells, the positions (*x*, *y* coordinates) of the center of every $CD11b^+$ cell and MC38GFP cell were first determined using CellProfiler. The distance between the center of every $CD11b^+$ and a given MC38GFP cell was then calculated in Excel, and the number of $CD11b^+$ within 40 μm of each MC38GFP cell was counted.

FACS Analysis. Lungs were collected and washed in PBS. The lungs were minced and digested with Collagenase/Dispase (Roche) at 37 °C. Cells were then passed through a 70-μm mesh, washed in FACS buffer [PBS, 1% BSA, 2% (vol/vol) FBS, 5 mM EDTA], blocked with anti-mouse CD16/CD32 antibody (93; BioLegend), and stained with fluorophore-conjugated antibodies [anti-mouse CD3ε (145-2C11), CD11b (M1/70), CD19 (6D5), CD45 (30-F11), Gr1 (RB6-8C5), Ly6C (HK1.4), Ly6G (1A8), NK1.1 (PK136; all from BioLegend), CD11c (HL3; BD Biosciences), and F4/80 (Cl:A3-1; AbD Serotec)]. FACS analysis was performed on a LSRII flow cytometer (BD Biosciences), and data were analyzed with FlowJo (Tree Star).

Platelet Preparation. Mouse blood was collected by cardiac puncture, and washed platelets were prepared as described previously (20, 58, 59). Where indicated, platelets (5×10^8 per mL) were activated with thrombin (5 U/mL) for 15 min at 37 °C. Activated platelets were then directly used in the assays. Alternatively, the supernatant (releasate) was separated by centrifugation at 2,800 × *g* for 7 min. Supernatants from resting platelets (5×10^8/mL), MC38GFP (5×10^5/mL), and resting platelets plus MC38GFP were also generated by incubating cells for 15 min at 37 °C and subsequently centrifuging at 2,800 × *g* for 7 min.

Leukocyte Chemotaxis Assay. Mouse blood was collected by cardiac puncture and red blood cells were lysed for 5 min in RBC Lysis buffer (155 mM NH_4Cl, 12 mM $NaHCO_3$, 0.1 mM EDTA). Leukocytes were then washed in FACS buffer, blocked with CD16/32 antibody (BioLegend), and stained with fluorophore-conjugated primary antibodies (anti-mouse CD45, CD11b, Ly6C, and Ly6G). Different combinations of MC38GFP cells and platelet fractions were added into the lower chamber of a ChemoTx chemotaxis system (Transwell filter with 5-μm pore size; Neuroprobe) as chemoattractants. Blocking antibodies were used at 150 μg/mL when used individually. For antibody combinations, 75 μg/mL of each antibody was used to keep the total concentration of antibodies constant across all conditions. Stained leukocytes were plated in the upper chamber. Both the upper and lower chambers contained RPMI. After 2 h, the content of the lower chamber was collected and mixed with propidium iodide (for cell viability) and Bright Count absolute counting beads (Invitrogen). Samples were then analyzed by FACS to determine the number of migrated $CD45^+CD11b^+Ly6G^+$ granulocytes. For each sample, the number of positive cells was normalized to the number of Bright Count absolute counting beads and reported relative to the number of migrated cells in wells containing MC38GFP plus platelets.

Cytokine Array. Purified platelets were incubated with MC38GFP cells or thrombin for 15 min at 37 °C. The samples were then centrifuged at 2,800 × *g* for 7 min to pellet platelets and tumor cells. The supernatant was centrifuged for a second time and equal volumes of each sample were loaded on RayBio G-Series Mouse Cytokine Antibody Arrays 1000, which allow the simultaneous detection of 96 mouse cytokines and chemokines. The glass arrays were processed according to manufacturer's instructions, and the fluorescence signal was analyzed using an Axon GenePix Scanner.

Statistics. Statistics were performed with the GraphPad Prism Software. Unpaired two-sided *t* test was used to compare means of two independent groups to each other, whereas one-way ANOVA followed by Tukey's post test was used to compare the means of more than two independent groups.

ACKNOWLEDGMENTS. We thank Sharon Wu and Hong Jia for technical assistance, members of the Hynes Laboratory for advice, and the microscopy and flow cytometry core facilities of the Koch Institute Swanson Biotechnology Center for technical support. This work was supported by funding from American Lebanese Syrian Associated Charities (M.L.), by the Ludwig Center for Molecular Oncology at Massachusetts Institute of Technology (MIT), by Koch Institute MIT National Cancer Institute Support Grant P30-CA14051, by National Cancer Institute Grants U54-CA126515/U54 CA163109 (principal investigator, R.O.H.), and by the Howard Hughes Medical Institute, of which R.O.H. is an investigator.

1. Zhang XH, et al. (2013) Selection of bone metastasis seeds by mesenchymal signals in the primary tumor stroma. *Cell* 154(5):1060–1073.
2. Joyce JA, Pollard JW (2009) Microenvironmental regulation of metastasis. *Nat Rev Cancer* 9(4):239–252.
3. Labelle M, Hynes RO (2012) The initial hours of metastasis: The importance of cooperative host-tumor cell interactions during hematogenous dissemination. *Cancer Discov* 2(12):1091–1099.
4. Qian BZ, et al. (2011) CCL2 recruits inflammatory monocytes to facilitate breast-tumour metastasis. *Nature* 475(7355):222–225.
5. Wolf MJ, et al. (2012) Endothelial CCR2 signaling induced by colon carcinoma cells enables extravasation via the JAK2-Stat5 and p38MAPK pathway. *Cancer Cell* 22(1):91–105.
6. Läubli H, Spanaus KS, Borsig L (2009) Selectin-mediated activation of endothelial cells induces expression of CCL5 and promotes metastasis through recruitment of monocytes. *Blood* 114(20):4583–4591.
7. Borsig L, Wong R, Hynes RO, Varki NM, Varki A (2002) Synergistic effects of L- and P-selectin in facilitating tumor metastasis can involve non-mucin ligands and implicate leukocytes as enhancers of metastasis. *Proc Natl Acad Sci USA* 99(4):2193–2198.
8. Chen Q, Zhang XH, Massagué J (2011) Macrophage binding to receptor VCAM-1 transmits survival signals in breast cancer cells that invade the lungs. *Cancer Cell* 20(4):538–549.
9. Lu X, et al. (2011) VCAM-1 promotes osteolytic expansion of indolent bone micrometastasis of breast cancer by engaging α4β1-positive osteoclast progenitors. *Cancer Cell* 20(6):701–714.

10. Läubli H, Stevenson JL, Varki A, Varki NM, Borsig L (2006) L-selectin facilitation of metastasis involves temporal induction of Fut7-dependent ligands at sites of tumor cell arrest. *Cancer Res* 66(3):1536–1542.
11. Huh SJ, Liang S, Sharma A, Dong C, Robertson GP (2010) Transiently entrapped circulating tumor cells interact with neutrophils to facilitate lung metastasis development. *Cancer Res* 70(14):6071–6082.
12. Slattery MJ, Dong C (2003) Neutrophils influence melanoma adhesion and migration under flow conditions. *Int J Cancer* 106(5):713–722.
13. Spicer JD, et al. (2012) Neutrophils promote liver metastasis via Mac-1-mediated interactions with circulating tumor cells. *Cancer Res* 72(16):3919–3927.
14. Granot Z, et al. (2011) Tumor entrained neutrophils inhibit seeding in the premetastatic lung. *Cancer Cell* 20(3):300–314.
15. Fridlender ZG, et al. (2009) Polarization of tumor-associated neutrophil phenotype by TGF-beta: "N1" versus "N2" TAN. *Cancer Cell* 16(3):183–194.
16. Gay LJ, Felding-Habermann B (2011) Contribution of platelets to tumour metastasis. *Nat Rev Cancer* 11(2):123–134.
17. Nieswandt B, Hafner M, Echtenacher B, Männel DN (1999) Lysis of tumor cells by natural killer cells in mice is impeded by platelets. *Cancer Res* 59(6):1295–1300.
18. Im JH, et al. (2004) Coagulation facilitates tumor cell spreading in the pulmonary vasculature during early metastatic colony formation. *Cancer Res* 64(23):8613–8619.
19. Karpatkin S, Pearlstein E, Ambrogio C, Coller BS (1988) Role of adhesive proteins in platelet tumor interaction in vitro and metastasis formation in vivo. *J Clin Invest* 81(4): 1012–1019.
20. Labelle M, Begum S, Hynes RO (2011) Direct signaling between platelets and cancer cells induces an epithelial-mesenchymal-like transition and promotes metastasis. *Cancer Cell* 20(5):576–590.
21. Schumacher D, Strilic B, Sivaraj KK, Wettschureck N, Offermanns S (2013) Platelet-derived nucleotides promote tumor-cell transendothelial migration and metastasis via P2Y2 receptor. *Cancer Cell* 24(1):130–137.
22. Daley JM, Thomay AA, Connolly MD, Reichner JS, Albina JE (2008) Use of Ly6G-specific monoclonal antibody to deplete neutrophils in mice. *J Leukoc Biol* 83(1):64–70.
23. Kowanetz M, et al. (2010) Granulocyte-colony stimulating factor promotes lung metastasis through mobilization of $Ly6G^{+}Ly6C^{+}$ granulocytes. *Proc Natl Acad Sci USA* 107(50):21248–21255.
24. Hodivala-Dilke KM, et al. (1999) Beta3-integrin-deficient mice are a model for Glanzmann thrombasthenia showing placental defects and reduced survival. *J Clin Invest* 103(2):229–238.
25. Kunita A, et al. (2007) The platelet aggregation-inducing factor aggrus/podoplanin promotes pulmonary metastasis. *Am J Pathol* 170(4):1337–1347.
26. Gasic GJ, Gasic TB, Stewart CC (1968) Antimetastatic effects associated with platelet reduction. *Proc Natl Acad Sci USA* 61(1):46–52.
27. Camerer E, et al. (2004) Platelets, protease-activated receptors, and fibrinogen in hematogenous metastasis. *Blood* 104(2):397–401.
28. Gasic GJ, Koch PA, Hsu B, Gasic TB, Niewiarowski S (1976) Thrombogenic activity of mouse and human tumors: Effects on platelets, coagulation, and fibrinolysis, and possible significance for metastases. *Z Krebsforsch Klin Onkol Cancer Res Clin Oncol* 86(3):263–277.
29. Honn KV, Tang DG, Crissman JD (1992) Platelets and cancer metastasis: A causal relationship? *Cancer Metastasis Rev* 11(3-4):325–351.
30. Gleissner CA, von Hundelshausen P, Ley K (2008) Platelet chemokines in vascular disease. *Arterioscler Thromb Vasc Biol* 28(11):1920–1927.
31. Zhang C, Gadue P, Scott E, Atchison M, Poncz M (1997) Activation of the megakaryocyte-specific gene platelet basic protein (PBP) by the Ets family factor PU.1. *J Biol Chem* 272(42):26236–26246.
32. Stadtmann A, Zarbock A (2012) CXCR2: From bench to bedside. *Front Immunol* 3:263.
33. Gil-Bernabé AM, et al. (2012) Recruitment of monocytes/macrophages by tissue factor-mediated coagulation is essential for metastatic cell survival and premetastatic niche establishment in mice. *Blood* 119(13):3164–3175.
34. Acharyya S, et al. (2012) A CXCL1 paracrine network links cancer chemoresistance and metastasis. *Cell* 150(1):165–178.
35. Ferjančič Š, et al. (2013) VCAM-1 and VAP-1 recruit myeloid cells that promote pulmonary metastasis in mice. *Blood* 121(16):3289–3297.
36. Kawamura M, et al. (2012) CXCL5, a promoter of cell proliferation, migration and invasion, is a novel serum prognostic marker in patients with colorectal cancer. *Eur J Cancer* 48(14):2244–2251.
37. Teramukai S, et al. (2009) Pretreatment neutrophil count as an independent prognostic factor in advanced non-small-cell lung cancer: An analysis of Japan Multinational Trial Organisation LC00-03. *Eur J Cancer* 45(11):1950–1958.
38. Lee YY, et al. (2012) Pretreatment neutrophil:lymphocyte ratio as a prognostic factor in cervical carcinoma. *Anticancer Res* 32(4):1555–1561.
39. Gondo T, et al. (2012) Prognostic value of neutrophil-to-lymphocyte ratio and establishment of novel preoperative risk stratification model in bladder cancer patients treated with radical cystectomy. *Urology* 79(5):1085–1091.
40. Chiang SF, et al. (2012) Can neutrophil-to-lymphocyte ratio predict the survival of colorectal cancer patients who have received curative surgery electively? *Int J Colorectal Dis* 27(10):1347–1357.
41. Proctor MJ, et al. (2012) A derived neutrophil to lymphocyte ratio predicts survival in patients with cancer. *Br J Cancer* 107(4):695–699.
42. Perez DR, et al. (2013) Blood neutrophil-to-lymphocyte ratio is prognostic in gastrointestinal stromal tumor. *Ann Surg Oncol* 20(2):593–599.
43. Shimada H, et al. (2004) Thrombocytosis associated with poor prognosis in patients with esophageal carcinoma. *J Am Coll Surg* 198(5):737–741.
44. Hwang SG, et al. (2012) Impact of pretreatment thrombocytosis on blood-borne metastasis and prognosis of gastric cancer. *Eur J Surg Oncol* 38(7):562–567.
45. Symbas NP, et al. (2000) Poor prognosis associated with thrombocytosis in patients with renal cell carcinoma. *BJU Int* 86(3):203–207.
46. Stone RL, et al. (2012) Paraneoplastic thrombocytosis in ovarian cancer. *N Engl J Med* 366(7):610–618.
47. Hernandez E, Lavine M, Dunton CJ, Gracely E, Parker J (1992) Poor prognosis associated with thrombocytosis in patients with cervical cancer. *Cancer* 69(12):2975–2977.
48. Ikeda M, et al. (2002) Poor prognosis associated with thrombocytosis in patients with gastric cancer. *Ann Surg Oncol* 9(3):287–291.
49. Stravodimou A, Voutsadakis IA (2013) Pretreatment thrombocytosis as a prognostic factor in metastatic breast cancer. *Int J Breast Cancer* 2013:289563.
50. Ishizuka M, Nagata H, Takagi K, Iwasaki Y, Kubota K (2013) Combination of platelet count and neutrophil to lymphocyte ratio is a useful predictor of postoperative survival in patients with colorectal cancer. *Br J Cancer* 109(2):401–407.
51. Holz O, et al. (2010) SCH527123, a novel CXCR2 antagonist, inhibits ozone-induced neutrophilia in healthy subjects. *Eur Respir J* 35(3):564–570.
52. Yang L, et al. (2008) Abrogation of TGF beta signaling in mammary carcinomas recruits $Gr\text{-}1^{+}CD11b^{+}$ myeloid cells that promote metastasis. *Cancer Cell* 13(1):23–35.
53. Ijichi H, et al. (2011) Inhibiting Cxcr2 disrupts tumor-stromal interactions and improves survival in a mouse model of pancreatic ductal adenocarcinoma. *J Clin Invest* 121(10): 4106–4117.
54. Bergmeier W, Rackebrandt K, Schröder W, Zirngibl H, Nieswandt B (2000) Structural and functional characterization of the mouse von Willebrand factor receptor GPIb-IX with novel monoclonal antibodies. *Blood* 95(3):886–893.
55. Nieswandt B, Bergmeier W, Rackebrandt K, Gessner JE, Zirngibl H (2000) Identification of critical antigen-specific mechanisms in the development of immune thrombocytopenic purpura in mice. *Blood* 96(7):2520–2527.
56. Ho-Tin-Noé B, Goerge T, Cifuni SM, Duerschmied D, Wagner DD (2008) Platelet granule secretion continuously prevents intratumor hemorrhage. *Cancer Res* 68(16): 6851–6858.
57. Lamprecht MR, Sabatini DM, Carpenter AE (2007) CellProfiler: Free, versatile software for automated biological image analysis. *Biotechniques* 42(1):71–75.
58. Frenette PS, Johnson RC, Hynes RO, Wagner DD (1995) Platelets roll on stimulated endothelium in vivo: An interaction mediated by endothelial P-selectin. *Proc Natl Acad Sci USA* 92(16):7450–7454.
59. Hartwell DW, et al. (1998) Role of P-selectin cytoplasmic domain in granular targeting in vivo and in early inflammatory responses. *J Cell Biol* 143(4):1129–1141.